Intersubband resonances and plasmons in quasi-two-dimensional systems: A line-shape and coupling analysis

D. H. Ehlers
Max-Planck-Institut für Festkörperforschung, Heisenbergstrasse 1, D-7000 Stuttgart 80, Federal Republic of Germany
(Received 20 April 1988)

Charge- and spin-density fluctuation spectra, as they appear in electron scattering and optical experiments, have been calculated for accumulation layers at *n*-type GaAs interfaces. Starting with a self-consistent ground state, we employ the random-phase approximation to evaluate the nonlocal susceptibility of the anisotropic electron system. Temperature effects and excitations to the continuum of states are also included in the theory. Profiles of the complex induced potential inside the quasi-two-dimensional (2D) electron gas reveal the internal structure of the collective modes. We find substantial deviations of the 2D plasmon dispersion from strictly two-dimensional theories. Both nonlocality and coupling between the subbands play a role. Also the dispersion of the intersubband resonance has been calculated over a wide range of wave vectors $q_{\parallel}$ and for various electron densities. The well-known depolarization shift at small $q_{\parallel}$ is strongly influenced by the spectral proximity of the continuum of states.

I. INTRODUCTION

Much interest recently has been devoted to the dynamics of quasifree electrons in semiconductor interface layers, both experimentally and theoretically. Especially the plasmons, the collective eigenmodes of the system, clearly reflect effects of dimensionality and nonlocality. They hence are key features in many investigations.

There are two distinct types of model systems: depletion layers, where the electron concentration only slowly reaches its bulk value, and accumulation layers, in which the carrier concentration considerably exceeds that deeper inside the crystal. The case of a carrier depletion is that most commonly found on free semiconductor surfaces, where electrons localized in surface states (dangling bonds, defects, etc.) repel their counterparts in the conduction band of the crystal. The dynamics of such depletion layers thus can be probed by means of high resolution inelastic electron scattering (HRELS) as has been proved by the pioneering experiments of Lüth and his co-workers.[1–4]

The opposite case of accumulation layers so far has been studied almost exclusively by optical means, mainly Raman scattering[5] or infrared absorption.[6,7] The reason is their larger experimental probing depth, and such layers easily can be formed by applying an external electric potential in metal-oxide-semiconductor-like structures or in heterostructures, where the band offset between two materials (e.g., GaAs-AlAs) naturally requires the build-up of accumulation layers

These kinds of inhomogeneous electron gases have one property in common: There is a long-range correlation between electronic excitations at different points of the structure, on the same length scale as the band bending itself. The dynamic response becomes strongly nonlocal.

In a previous publication[8] we presented a theoretical description of the dynamics in such systems. The numerical part of that work concentrated on surface plasmons on GaAs at room temperature, the parameter regime corresponding to most existing HRELS data. In this paper we now want to focus on accumulation layers at lower temperatures. With temperatures decreasing from 300 K to a few kelvin there should be a continuous transition from an inhomogeneous, but semi-infinite electron gas to a quasi-two-dimensional system, due to the freeze out of free carriers in the bulk. The initial interface plasmon will develop to a truly quasi-two-dimensional mode, with its amplitude localized just as the electrons in the two-dimensional subbands are. Also the Landau damping is expected to change drastically.

In the field of two-dimensional electron gases there has been a lot of theoretical work on systems, where only one or a small number of subbands play a role.[9] These theoretical models are applicable at most to inversion layers, where the occupied subbands are far below the conduction-band edge of the bulk. For accumulation layers, however, there is a continuum of states energetically close to the subbands, and this will be shown to be of considerable importance. Its influence is most apparent in the well-known depolarization shift of the intersubband resonances.

The emphasis of this paper will be on wave-vector transfers beyond the better known long-wavelength limit. In this regime the nonlocal coupling mechanisms between different excitation modes should become important. The present formulation allows us to take into account intersubband transitions and two-dimensional plasmons on the same footing, based on a self-consistent ground state. We then calculate both spin-density and charge-density fluctuation spectra, with full information on oscillator strength and line shapes. Additionally, dynamic potential profiles reveal some new insight in excitations of two-dimensional systems.

The outline of this paper is as follows: In Sec. II we re-

view the theoretical approach and summarize the relevant quantities. The numerical results for a wide range of accumulation electron densities and wave-vector transfers then will be discussed in Sec. III, and we summarize our conclusions in Sec. IV.

II. THEORETICAL MODEL

As in our previous publication[8] we will present the results by calculating a microscopic structure factor which directly determines experimental spectra. The basic concept and definitions needed in this work will be given briefly.

We apply a semi-infinite geometry with the interface at $z=0$ and the electron gas of interest in the upper half-space ($z>0$). The crystal is assumed to be sufficiently thick so that bulk behavior is realized for large z. For heterostructures this requires the total layer thickness to be larger than the extent of the accumulation and that of the dynamic potential associated with any of its excitations considered. Further, the model system is translationary invariant parallel to the interface plane, and hence all quantities are characterized by their (parallel) wave vector $q_\parallel$.

We are now interested in the collective excitations of the quasi-free electrons. They are part of the spectrum of the charge-density fluctuations $\delta\rho(q_\parallel,z,t)$, given by

$$\int_{-\infty}^{\infty}\frac{dt}{\hbar}e^{-i\omega t}\langle\delta\rho^{\dagger}(q_\parallel,z,t)\delta\rho(q_\parallel,z',0)\rangle = 2[1+N(\omega)]\,\mathrm{Im}\chi(q_\parallel,\omega,z,z')\ , \quad (2.1)$$

where $\langle\ \rangle$ denotes the statistical average of the ensemble at temperature T,

$$N(\omega)=[\exp(\hbar\omega/k_BT)-1]^{-1}\ ,$$

the Bose-Einstein function, and the susceptibility χ is the Fourier transform of the retarded Green's function of the density operator. We will calculate $\chi(q_\parallel,\omega,z,z')$ within the random-phase approximation (RPA). Local-field corrections could of course be included in this self-consistent-field scheme employing the local-density approximation of the density-functional approach, but for strongly inhomogeneous systems its reliability is still unclear. This remains true even when temperature[10,11] and frequency dependence[12] are taken into account. Also local-field effects can be estimated to yield only a modest correction, in the 5% range for GaAs,[13,14] and calculating the response within the RPA allows us to compare certain features directly with simpler theories.

Corresponding to the RPA for the susceptibility, the ground-state envelope wave functions that enter the theory are calculated from a self-consistent Hartree potential. A major ingredient of our scheme is the use of a parametrization[15] that yields analytic expressions for all wave functions and one-particle Green's functions needed in the theory. Details of the formalism and also on the numerical procedures can be found in previous publications.[16,8]

The charge-density fluctuations $\delta\rho$ are directly probed in the dipole scattering regime of electron energy-loss spectroscopy[17] (HRELS) and in electronic Raman scattering with parallel polarization.[18] It also dominates the absorption in infrared spectroscopy.[19,20]

In HRELS the differential scattering efficiency may be written as[21]

$$\frac{dS(\omega)}{d\hbar\omega}=\frac{e^2}{2\pi}\int d^2q_\parallel g^2(q_\parallel,\omega)\frac{1}{q_\parallel^2}P(q_\parallel,\omega)\ , \quad (2.2)$$

where the kinematic factor $g(q_\parallel,\omega)$ is the Fourier transform of the Coulomb potential $1/|\mathbf{v}t|$ of the scattered electron with velocity $\mathbf{v}$. The boundaries of the integration over $\mathbf{q}_\parallel$ are determined by the acceptance angle of the analyzer. $P(q_\parallel,\omega)$ is the "structure factor" of the system. Employing Eq. (2.1) it can be written as

$$P(q_\parallel,\omega)=\frac{8e^2}{|\epsilon_A+\epsilon_B|^2}\times\int_0^\infty dz\int_0^\infty dz'e^{-q_\parallel(z+z')}\times[1+N(\omega)]\mathrm{Im}\chi(q_\parallel,\omega,z,z')\ , \quad (2.3)$$

where ϵ_B is the background dielectric constant of the medium the quasifree electrons are embedded in, and ϵ_A is the one on the other side of the interface ($z<0$), e.g., vacuum or GaAlAs.

It is worth mentioning that a similar weighting of the bilocal fluctuation spectrum occurs in the Raman cross section for primary photon energies above the absorption edge,[22] and also for the main contribution to infrared absorption.[23] Thus we chose the structure factor P to be the key quantity in our numerical analysis.

Only in the long-wavelength limit $q_\parallel\to 0$ and under certain additional assumptions $P(q_\parallel,\omega)$ can be shown[8] to reduce to the well-known "surface" loss function of macroscopic dielectric theory,

$$\lim_{q_\parallel\to 0}P(q_\parallel,\omega)=\frac{2q_\parallel}{\pi}[1+N(\omega)]\mathrm{Im}\frac{-1}{\epsilon_T+\epsilon_A}\ , \quad (2.4)$$

with $\epsilon_T=\epsilon_B-\omega_p^2/\omega^2$ and $\omega_p^2=4\pi n(\infty)e^2/m$, the plasma frequency in the bulk. This limit does not remain valid for strong accumulation layers at sufficiently low temperatures, where subband binding energies exceed $\hbar\omega_P$. (Note that ω_P of course is zero for a truly quasi-to-dimensional electron gas.) Exactly such accumulation layers are of interest in the present work and even for small $q_\parallel$ employing the fully microscopic and nonlocal susceptibility is essential.

III. RESULTS AND DISCUSSION

All numerical results of this work refer to n-type gallium arsenide, which not only is one of the experimentally best studied semiconductors, but also shows only small effects of nonparabolicity of the conduction band. In our model calculations we therefore employed the parabolic approximation. Then the only crystal parameters that enter the theory are the effective mass $m=0.069m_e$ and

the background dielectric constant $\epsilon_B = \epsilon_\infty = 10.9$.[24] For the adjacent medium we chose—if not otherwise stated—$\epsilon_A = 1$ of the vacuum. The contribution from the optical phonons of GaAs and their coupling to the electronic excitations are omitted for clarity. At this stage our interest lies in the microscopic response of the unperturbed electron system. We have demonstrated in a previous publication, however, how to fully incorporate the longwavelength optical phonons into the theory.[8]

Further, in the numerical work the doping concentration is taken to be 1.3×10^{17} cm^{-3}, independent of temperature. This corresponds to a bulk carrier concentration of 1.0×10^{17} cm^{-3} at $T=300$ K and 1.6×10^{13} at 5 K. We then can study temperature effects similar to those that would appear in an experiment. This is demonstrated in Fig. 1, where we plot $P(\omega)$ (solid line) for constant accumulation charge and constant wave vector $q_\parallel$, but varying temperature. $q_\parallel = 0.005$ Å$^{-1} = 5\times10^5$ cm^{-1} is a value typical for electron energy-loss spectroscopy, but slightly larger than values attainable in Raman or ir spectroscopy. With decreasing temperature the main feature of the spectrum sharpens considerably and moves to lower frequencies. At the same time a clearly resolvable second peak emerges at its high-frequency shoulder. It is due to collective intersubband transitions, often labeled as intersubband plasmon. They will be discussed in more detail below.

At $T=300$ K the system is constituted by a half-bound electron gas, with an inhomogeneity due to the accumulation close to the interface. Hence at small $q_\parallel$ the spectral feature may be labeled as interface plasmon, only with its intensity and frequency enlarged by the accumulation charge. Also the plasmon is broadened by the strong Landau damping. This kind of excitation has been extensively studied in our earlier work.[8] With decreasing temperature the Landau damping reduces and the quasifree carriers in the bulk are freezed out. There is a continuous transition to a quasi-two-dimensional (2D) plasmon in the accumulation layer.

The dotted curves in Fig. 1 are the corresponding spin-density fluctuation spectra as they can be observed experimentally in Raman scattering with crossed polarization.[18] In the spirit of the RPA they here are calculated by setting the Coulomb potential between charge-density fluctuations identical to zero. The susceptibility $\chi(q_\parallel,\omega,z,z')$ is replaced by the pure irreducible electron-hole propagator $\chi_0(q_\parallel,\omega,z,z')$.[8] The curves thus reveal the excitation spectra of single electron-hole pairs (sp).

At 300 K there is a broad continuum characteristic of an almost classical Boltzmann gas, which with decreasing temperature changes to the spectrum of degenerate two-dimensional system. The sharp cutoff occurs at

$$\hbar\omega = \hbar^2(2k_{F1}q_\parallel + q_\parallel^2)/2m \ ,$$

when k_{F1} is the Fermi wave vector of the electrons in the lowest subband. At even higher frequencies there are the intersubband transitions. Compared to their broad sp spectrum, that of the (screened) charge-density fluctuations between the subbands is much sharper. This spectral sharpness of course is a characteristic of any well-defined collective mode.

Differences between charge- and spin-density spectra, as they are shown in Fig. 1, had been observed in many Raman experiments.[5] It should also be mentioned, however, that even the line shape and intensity of the intersubband resonance relative to the 2D plasmon is very similar to those found in grating induced infrared absorption.[6] This supports the fact that in ir spectroscopy the longitudinal susceptibility χ is dominating. Also the experimental weightening of the nonlocal response function in the structure factor P [Eq. (2.3)] is an appropriate description for ir absorption at least in the grating coupler geometry.

In Fig. 2 the temperature dependence of some of the

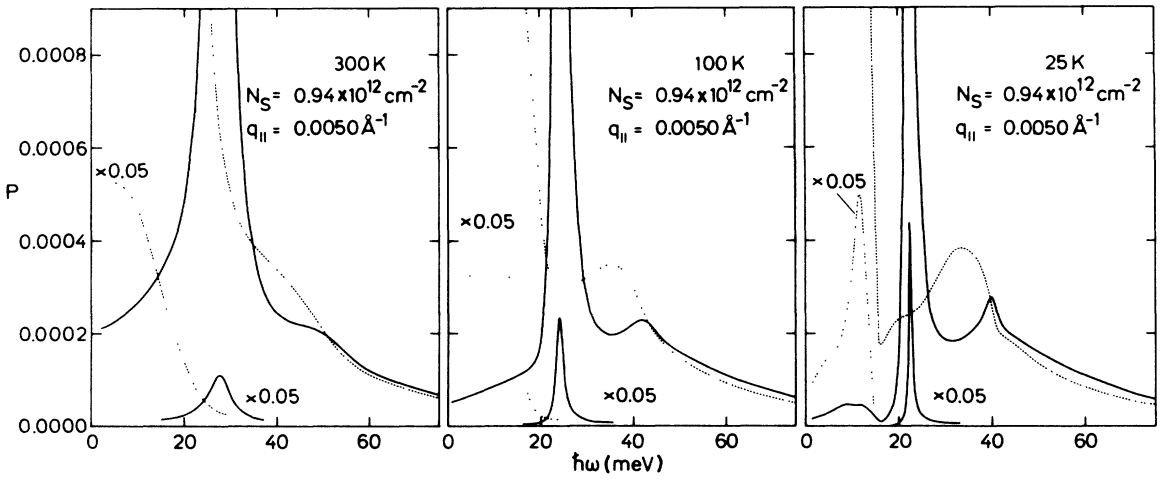

FIG. 1. For three different temperatures we plot the structure factor $P(\omega)$ [Eq. (2.3)] in units of $2me^2/\hbar^2$ for charge-density fluctuations (——) and spin-density fluctuations (· · · ·). We consider GaAs with the doping concentration $n_D = 1.3\times10^{17}$ cm^{-3} and the accumulation density and wave vector indicated. The solid curves show the plasmon (main feature) and at higher frequencies the less intense intersubband resonance.

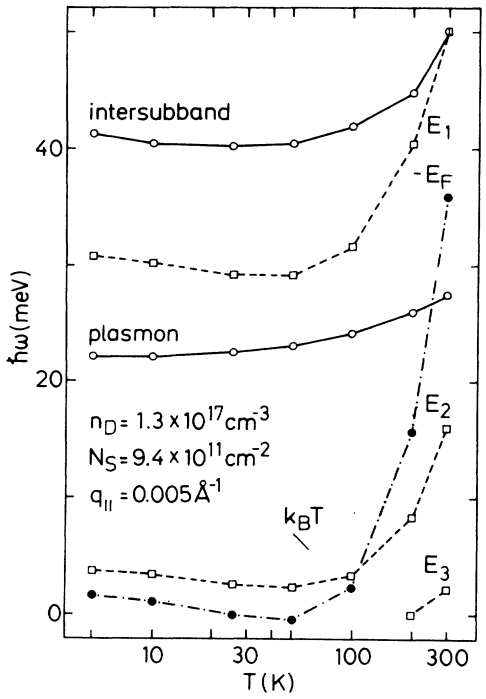

FIG. 2. Temperature dependence of some characteristic energies in GaAs accumulation layers. The doping again is 1.3×10^{17} cm^{-3}. We show collective modes (——) as obtained from the maxima of $P(\omega)$, $-E_F$, and the subband binding energies (relative to the bulk conduction-band edge) for the accumulation N_S indicated.

relevant energies is summarized for the accumulation charge N_S indicated: those of the (interface) plasmon and the collective intersubband transition ($\hbar\tilde{\omega}_{12}$), the binding energies E_1, E_2, and E_3 of the subbands and the distance of the Fermi energy from the bulk conduction-band edge ($E=0$). For $T<200$ K the accumulation layer becomes so narrow that only two subbands survive, and at even lower temperature E_1, E_2, and $\hbar\tilde{\omega}_{12}$ follow the slope of E_F. The plasmon characterized by its density fluctuation parallel to the interface instead monotonically moves to lower frequencies, indicating the continuous transition to the 2D plasmon. For $T\lesssim25$ K the electron density in the accumulation layer exceeds that in the bulk by more than 2 orders of magnitude and standard criteria for two dimensionality are fulfilled. In what follows we therefore restrict our numerical calculations to that temperature.

In Fig. 3 again the structure factor $P(\omega)$ is plotted, showing the charge-density fluctuation spectra (solid line) and those of the spin density (dotted line), now for two accumulation densities N_S and three wave vectors $q_{||}$. The frequency of the 2D plasmon increases both with N_S and $q_{||}$, as expected. However, different from the interface plasmon at 300 K,[8] it does not show increasing Landau damping. In contrast it even gains intensity at larger $q_{||}$ as can be understood from an analysis of the f sum rule:[8,25] For localized (2D) systems the effective number of electrons decreases less than proportional to $1/q_{||}$, and for a dispersion less than proportional to $q_{||}$ the intensity should increase. The length scale of the screening Coulomb interaction better fits the extent of the accumulation layer at larger $q_{||}$, and hence the buildup of the collective mode is more efficient.

The absence of noticeable Landau damping can be understood by direct comparison with the pair excitation spectra. Even for $q_{||}=0.01$ Å^{-1} the intrasubband sp excitations still lie energetically below the plasmon and therefore do not constitute a "decay channel."

This is different for the collective intersubband resonance. It not only shows strong dispersion, but also strong damping. The energetic overlap with the intersubband sp spectrum increases with $q_{||}$, and for $q_{||}=0.01$ Å^{-1} the collective mode can be seen only as a broad shoulder of the 2D plasmon. Again, such large wave-vector transfers are not directly achievable in *optical* spectroscopy. Similar systematic broadening has only been observed with increasing impurity scattering in resonant Raman spectroscopy.[26]

In the spin-density fluctuation spectra there are considerable differences for the two accumulation densities. For $N_S=1.4\times10^{12}$ cm^{-2} there is additional structure in both the low-energy intrasubband excitations and in the intersubband features. In the intrasubband spectrum there now are two peaks corresponding to the cutoffs of the independent electron gases in the two subbands. For this large accumulation also the second subband is sufficiently populated. Its Fermi wave vector k_{F2} amounts to almost one-third of that of the lowest subband.

Also the intersubband excitations now show two maxima. They correspond to excitations where the wave vector of the final electron state is parallel or antiparallel to $\mathbf{q}_{||}$, respectively. The spectrum splits due to the population of the upper subband. As is illustrated in Fig. 4, in one dimension there would be an excitation gap which in two dimensions survives in the density of states. The maxima should occur at $E_{12}\pm\hbar^2(k_{F1}+k_{F2})q_{||}/2m$. In the complete spectra, however, they appear at slightly larger frequencies. This is due to the superimposed transitions into the continuum of states above the mobility edge. Double structures which clearly reveal information on the population of the upper subband have not yet been reported from experiments.

In the following two figures we show spatial profiles of the induced electric potentials $\phi_{\rm el}^{\rm ind}(z)$ at various excitation frequencies. $\phi_{\rm el}^{\rm ind}$ is the potential generated by the charge fluctuations of the electron system, given by

$$\phi_{\rm el}^{\rm ind}(q_{||},\omega,z)=-\int_0^\infty dz'\int_0^\infty dz'' v(q_{||},\omega,z,z') \times\chi(q_{||},\omega,z',z'') \times\phi_B^{\rm ext}(q_{||},\omega,z'') , \quad (3.1)$$

with $\phi_B^{\rm ext}=\phi^{\rm ext}/\epsilon_B$ the screened external potential and v the Coulomb potential. The external potential is chosen Coulomb-like, so that its Fourier coefficient is exponentially decaying inside the layer: $\phi^{\rm ext}\sim\exp(-q_{||}z)$. This is shown in the inset of Fig. 5 together with the static density profile of the system and its contribution from the

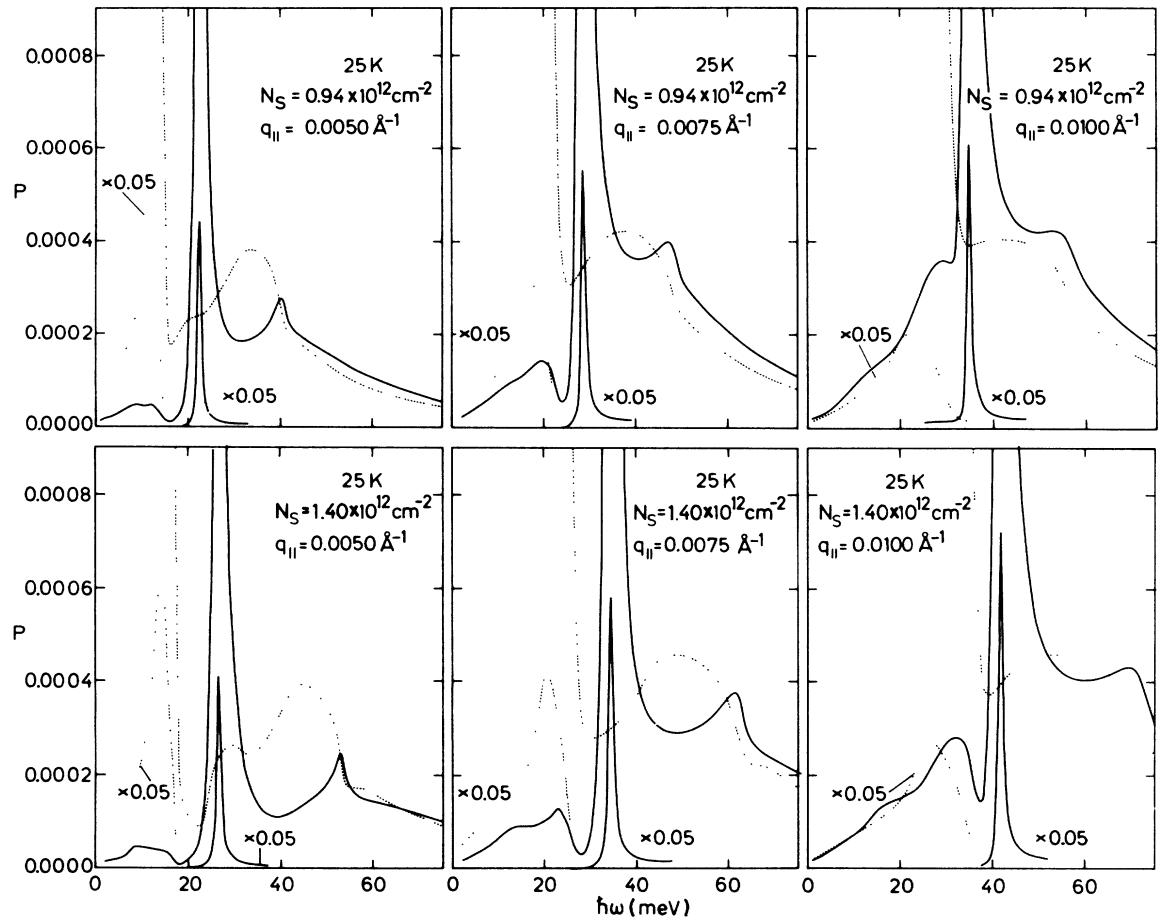

FIG. 3. The spectral function $P(\omega)$ as in Fig. 1, but now for constant low temperature and different accumulation densities N_S and wave vectors $q_{||}$. Again we plot charge-density (——) and spin-density-fluctuation spectra (· · · ·). The main peak in solid curves (——) is due to the 2D plasmon, and the less intense feature at higher frequencies reflects the intersubband resonance.

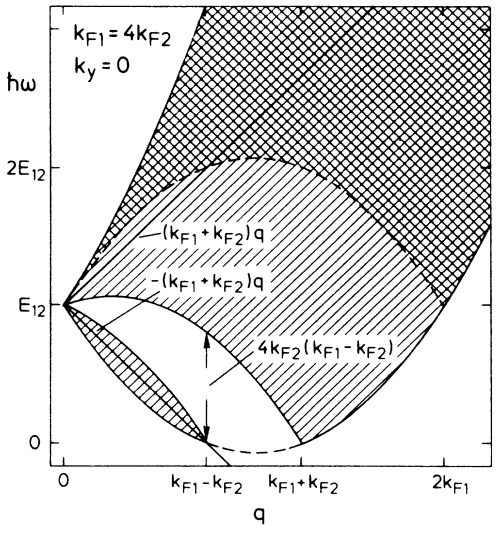

FIG. 4. Pair excitation spectrum for intersubband transitions in an one-dimensional electron gas ($k_y = 0$). E_{12} is the difference of the subband binding energies and k_{F1} and k_{F2} are their Fermi wave vectors. We also show the corresponding intrasubband excitations with $E_{12} \equiv 0$, $k_{F1} = k_{F2}$ (cross hatched). Within the figure energies are given in units of $\hbar^2/2m$.

second subband. For $q_{||} = 0.005$ Å^{-1} we have $\phi^{exp} \simeq (1 - q_{||} z)$ inside the accumulation layer, and the external electric field almost constant. It is a long-wavelength excitation on this length scale.

In the main part of Fig. 5 we then plot the absolute value of $\phi^{ind}_{el}(z)/\phi^{ext}_B(z)$, which can be interpreted as effective quasilocal response $(\epsilon_T^{-1} - \epsilon_B^{-1})\phi^{ext}_B$ of the electron system, $\epsilon_T = \epsilon_B/(1 - v\chi)$ being the total nonlocal dielectric function in the RPA.

At the plasmon resonance ($\hbar\omega_{2D} = 29$ meV) of course also the corresponding potential becomes very large, and we thus show profiles only well below and above this frequency. For any frequency below the intersubband resonance $\hbar\tilde{\omega}_{12} = 53$ meV the response has its maximum deep inside the crystal, considerably deeper than the static (see inset) and also induced densities. The shape of the profile then changes drastically at this intersubband resonance frequency, with the induced potential now being largest close to the interface.

Deep inside the crystal the absolute value of the induced potential shows oscillations, whose period decreases with increasing frequency. Qualitatively they are independent of $q_{||}$ and unchanged also in the absence of

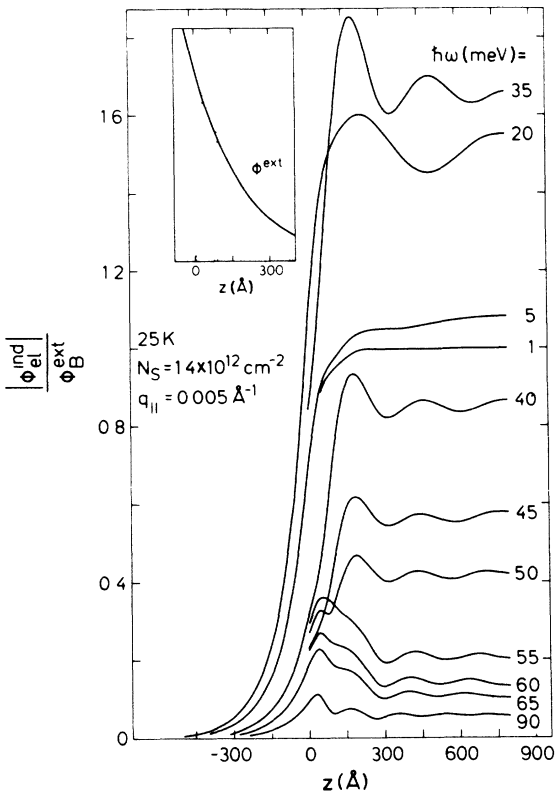

FIG. 5. We plot profiles of the absolute value of the effective local susceptibility $\phi_{\rm el}^{\rm ind}/\phi_B^{\rm ext}(z)$ (see text) for $\phi^{\rm ext}\sim\exp(-q_\parallel z)$ and various excitation frequencies. The static electron density profile and its contribution from the second subband, together with the external potential, are shown in the inset.

image charge effects ($\epsilon_A \equiv \epsilon_B$). The oscillations also show different behavior than those found for metal surfaces.[27,28] Here they must be due to the real-space cutoff, i.e., the localization of the quasi-two-dimensional electron gas. [Note, however, that an exponential decay $\sim\exp(-q_\parallel z)$ of $\phi_{\rm el}^{\rm ind}$ is superimposed; $|\phi_{\rm el}^{\rm ind}|/\phi_B^{\rm ext}$ is plotted.]

The phase of the complex $\phi_{\rm el}^{\rm ind}$ relative to $\phi^{\rm ext}$ is shown in Fig. 6, again for an exponentially decaying external potential. Here the profiles for various frequencies are given in the inset, showing oscillations of decreasing wavelength similar to those of the absolute value (Fig. 5). The dotted line again indicates the position of the static density profile and its contribution from the second subband. In the region of the accumulation layer the phase changes drastically, before starting the oscillations further inside. On the contrary, for the half-bound electron gas in our earlier work[8] we found a monotonically increasing phase. This we interpreted as a bulk-plasmon wave launched from the interface layer, which of course is not possible in the 2D geometry.

In the main part of Fig. 6 we show the phase φ as a function of frequency at various depths z, similar to a topograpic plot. Below the 2D plasmon frequency ($\hbar\omega_{\rm 2D}=29$ meV) there is only little dependence of φ on z and only $\varphi\ (z=0)$ is shown. At the resonance there is a phase "jump" from $-\pi$ to 0, which due to the strong localization is much more pronounced than in the half-bound geometry.[8] Above $\omega_{\rm 2D}$ the phases at different depths start to spread, indicating "vertical" excitations, i.e., charge oscillations perpendicular to the interface. Those are transitions between the spatially separated subbands as could be seen directly from the induced densities. They show two distinct maxima, each out of phase from the other, and for sufficiently small $q_\parallel$ just at the maxima of the static subband densities (inset).

The major feature of the plot, however, is the phase jump at $\hbar\omega=53$ meV, that frequency where the intersubband resonance shows up in the dynamic structure factor P (Fig. 3) and the induced density has a relative maximum. This phase jump has to be interpreted as characteristic of the intersubband *plasmon*, opposed to the broad spectrum of intersubband pair excitations.

The collective mode is even more pronounced at yet smaller wave vectors $q_\parallel$, while at intermediate $q_\parallel$ the nonlocal coupling to all intrasubband and intersubband excitations causes more complicated dynamic density and potential profiles. The collective modes then can be most clearly identified by its phase behavior.

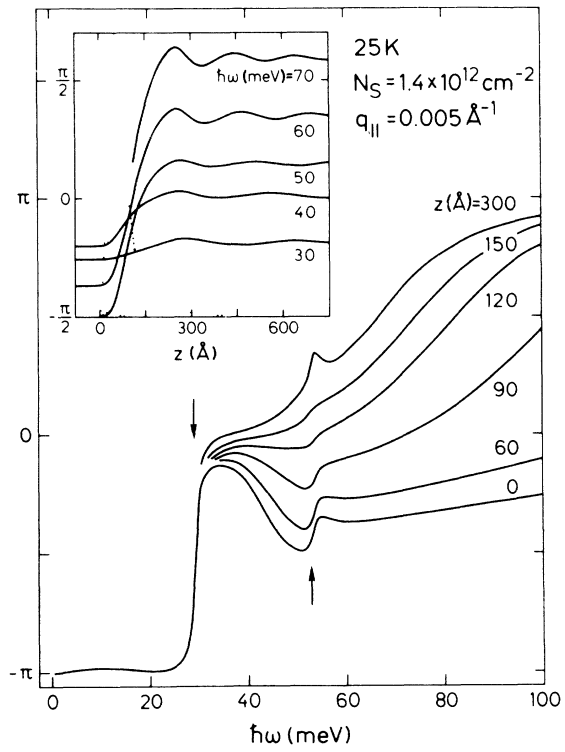

FIG. 6. The relative phase of the complex induced potential $\phi_{\rm el}^{\rm ind}$ [Eq. (3.1)] at various depths of the layer, as in Fig. 5 for an external excitation $\phi^{\rm ext}\sim\exp(-q_\parallel z)$. The arrows indicate the frequencies of the intrasubband and intersubband plasmons as found in the full function $P(\omega)$. In the inset we plot the phase profiles of $\phi_{\rm el}^{\rm ind}$ together with the static densities in the subbands (. . . .).

We now focus on the dispersion of the collective modes as they are found from the maxima in the charge-density-fluctuation spectra. In Fig. 7 the frequencies of the intrasubband and intersubband plasmons are plotted as a function of the parallel wave vector $q_\parallel$ and for three accumulation densities. The dotted lines indicate the upper edges of the sp spectra at $T=0$ K. That of intrasubband excitations is shown for $N_S=9.4\times10^{11}$ cm^{-2} only. The dashed lines are the dispersion curves of the 2D plasmon given by the approximate RPA formula by Chaplik,[29]

$$\omega_{2D}^2=\frac{2\pi e^2}{m\epsilon_{\text{eff}}}N_S(q_\parallel)\frac{(2+a_{\text{eff}}q_\parallel)^2}{4+a_{\text{eff}}q_\parallel}\ , \tag{3.2}$$

with $\epsilon_{\text{eff}}=\epsilon_B$, and a_{eff} then is the effective Bohr radius. Equation (3.2) reduces to the better known result by Stern[30] for small $q_\parallel$.

There are considerable differences between the frequencies according to Eq. (3.2) and those found here in the full spectra. First ϵ_{eff} is strongly dependent on $q_\parallel$ due to the finite extent of the accumulation and image charge effects,[31,32,7] and second the formula [Eq. (3.2)] neglects any intersubband transitions and their coupling to the plasmon.[33]

For small $q_\parallel$ the deviations are mainly due to our choice $\epsilon_{\text{eff}}=\epsilon_B$ in Eq. (3.2). Asymptotically it should be $\epsilon_{\text{eff}}(q_\parallel\to0)=(\epsilon_A+\epsilon_B)/2$, and $\hbar\omega$ should lie above the dashed line by almost a factor of $\sqrt{2}$. For finite $q_\parallel$, however, the values agree much better, thus reflecting the localization of the plasmon inside the accumulation layer. The dielectric constant ϵ_B is dominating.

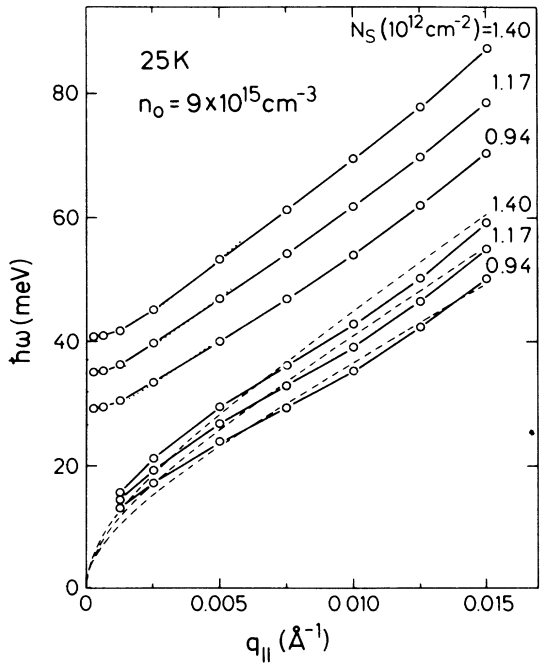

FIG. 7. For three accumulation densities we plot dispersion curves of the intrasubband and intersubband plasmons as obtained from the maxima of $P(q_\parallel\omega)$, and ω_{2D} according to Eq. (3.2) (— — —). The dotted lines show the upper edges of the corresponding pair excitation spectra (see text).

For $q_\parallel\gtrsim0.006$ Å^{-1} the maxima of the structure factor lie even below the dashed curves, and this deviation has to be ascribed to the repelling coupling to the intersubband resonance. When the calculation is repeated for $\epsilon_A=\epsilon(\text{AlAs})=8.16$, image charge effects are much smaller and the bare repulsion proves to be even larger than directly seen in the figure.

For the largest wave vectors considered here the plasmon just merges into the sp spectrum and only here strong Landau damping becomes possible. The line shape becomes very asymmetric similar to the interface plasmon of the half-bound electron gas.[8] On the contrary the intersubband plasmon is damped already for $q_\parallel$ as small as 0.005 Å^{-1}, where the dispersion curves intersect the upper edge of the sp spectra. For very large $q_\parallel$ the mode looses its collective character.

For $q_\parallel\to0$ the intersubband plasmon shows a quadratic dispersion[34] and the well-known depolarization shift. Its energy $\hbar\tilde{\omega}_{12}$ lies considerably above the subband spacing E_{12}, which is the onset of the dotted curves in Fig. 7. Ignoring so called nondiagonal coupling[19] and transitions to other than the second subband the resonance frequency should be given by[19]

$$\hbar^2\omega_{12}^2(q_\parallel\to0)=E_{12}^2(1+2\Delta_{12})\ , \tag{3.3a}$$

with the relative depolarization shift

$$\Delta_{ij}=N_S^{(ij)}V_{ijij}/E_{ij} \tag{3.3b}$$

and the Coulomb matrix elements

$$V_{klmn}=\int_0^\infty dz\int_0^\infty dz'\psi_k(z)\psi_l(z)v(q_\parallel\to0;z,z')\times\psi_m(z')\psi_n(z')\ . \tag{3.3c}$$

$N_S^{(ij)}$ is the difference[35] of the electron densities in the two subbands i and j, and v again is the Coulomb potential. The matrix elements V_{1212} when calculated explicitly for $q_\parallel=0$ can be interpreted as dipole length of the intersubband transition.

For comparison with the full model employed in this work some of the parameters are listed in Table I. From its last two lines we see that Eq. (3.3a) gives a depolarization shift almost twice as large as that found from the full density-fluctuation spectrum ($\hbar\tilde{\omega}_{12}$). For a more detailed understanding we hence also calculated V_{1c1c} and Δ_{1c}, the parameters as given by Eq. (3.3), but with $j\equiv c$ now being the continuum of conduction-band states with $E>0$, instead of the second discrete subband. The quantities thus are integrated values. V_{1c1c} gets its biggest contribution from a state with $E_j=+7.5$ meV (for $N_S=9.4\times10^{11}$ cm^{-2}), but the effective conduction-band energy as it can be extracted from the ratio V_{1c1c}/Δ_{1c} lies considerably higher.

It should be mentioned that we are able to calculate the matrix elements to the continuum quite efficiently, since with the ground-state parametrization employed (see Sec. II) we have *all* envelope functions ψ at hand

TABLE I. For three accumulation densities we list its contributions $N_S^{(1)}$ from the lowest subband, its binding energy and distance to the second subband, the Coulomb matrix elements V and relative depolarization shifts Δ (see text), and the model resonance frequency ω_{12} according to Eq. (3.3). For comparison we also show the frequency $\tilde{\omega}_{12}$ derived from the maxima of the full function $P(\omega)$.

N_S (10^{12} cm^{-2})	0.94	1.17	1.40
$N_S^{(1)}$ (10^{12} cm^{-2})	0.86	1.04	1.22
$\lvert E_1 \rvert$ (meV)	29.2	35.9	42.3
E_{12} (meV)	26.7	32.0	37.0
V_{1212} (10^{-12} meV cm^2)	6.67	6.63	6.49
V_{1112} (10^{-12} meV cm^2)	−28.0	−26.5	−25.1
V_{1c1c} (10^{-12} meV cm^2)	24.6	22.2	20.4
Δ_{12}	0.195	0.190	0.184
Δ_{1c}	0.270	0.243	0.224
Δ_{2c}	−0.530	−0.512	−0.370
$\hbar\omega_{12}$ (meV)	31.5	37.6	43.3
$\hbar\tilde{\omega}_{12}$ (meV)	29.2	35.0	40.6

analytically. Also exactly the same functions are used in the calculation of the full χ.[8]

Δ_{1c} and also Δ_{2c} are not quantities of the simple two-band model employed in Eq. (3.3), but they should yield some qualitative estimate of the relevance of the continuum. V_{1c1c} is much larger than V_{1212}, both decreasing with increasing energetic distance of the electronic states, but the Δ's remain balanced and comparable in size. It hence may be concluded, that in accumulation layers, where the second subband is not too far from the mobility edge, there does not exist a distinct mode for collective transitions between the two subbands only. Instead all transitions from the lowest subband are coupled and screen each other. They together determine the depolarization shift. There also is only one intersubband resonance in the charge-density spectrum, since even for $q_\parallel \to 0$ the spectrum of transitions to the continuum is broad. Allen *et al.*[36] performed a model calculation with a third relaxationlike broadened subband. They also found only one resonance with a lowered depolarization shift.

Finally in Fig. 8 we plot the frequencies of intersubband resonance and 2D plasmon as a function of accumulation density N_S. Also shown is ω_{2D} according to Eq. (3.2) and the subband binding energies.

For $N_S \gtrsim 3\times10^{11}$ cm^{-2} the plasmon frequencies as derived from the structure factor $P(\omega)$ follow that of the simple 2D theory quite well. The degree of agreement of the absolute values varies strongly with $q_\parallel$ (see Fig. 7), but the $\sqrt{N_S}$ dependence is remarkable. It indicates, that the 2D plasmon is a collective charge-density oscillation in *all* occupied states. This remains true even for large N_S, where a considerable contribution comes from the second subband. In that sense the nomenclature commonly applied, namely that of an *intra*subband

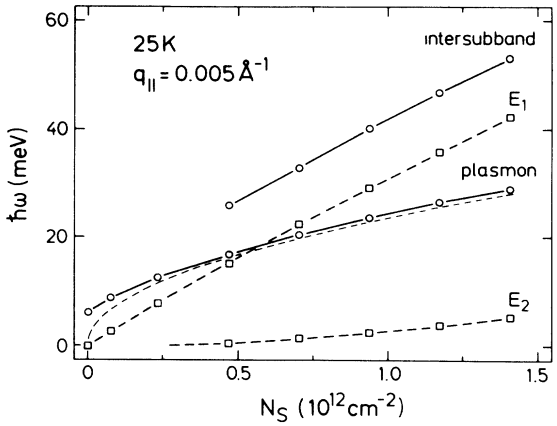

FIG. 8. Energies of the parallel plasmon and the intersubband resonance as a function of accumulation density. We also plot ω_{2D} from Eq. (3.2) (— — —) and the subband *binding* energies (———)

plasmon, is slightly misleading. The strong coupling between the subbands again leads to the buildup of a single mode.

The deviation from Eq. (3.2) at small densities N_S is due to the finite bulk density at 25 K and its corresponding quasiaccumulation.[16] The plasmon there can be described as an interface mode which, however, vanishes for large N_S. At fixed wave vector $q_\parallel = 5\times10^5$ cm^{-1} the frequencies of the 2D plasmon and the collective intersubband mode come close for $N_S \lesssim 5\times10^{11}$ cm^{-2}. The resulting coupling,[37] however, is not very apparent. It cannot be studied in detail from an analysis of $P(\omega)$ because of the comparatively small oscillator strength of the intersubband mode.

Finally, the parallel slope of the intersubband resonance $\tilde{\omega}_{12}$ and the binding energy E_1 of the lowest subband should be commented on. Opposed to Eq. (3.3) $\tilde{\omega}_{12}$ is not proportional to $\lvert E_1 - E_2 \rvert$ (compare also Fig. 2). At finite $q_\parallel$ the strong coupling into the continuum leads to a resonance between $-E_1$ and an effective upper state, which does not depend on N_S or E_2. For $q_\parallel \to 0$, however, the second subband dominates and $\hbar\tilde{\omega}_{12}$ is clearly smaller than the binding energy E_1 (Table I). The resonance hence ought to be labeled inter*sub*band.

IV. CONCLUSION

For accumulation layers and wave vectors beyond the better known long-wavelength limit we have calculated charge-density and spin-density fluctuation spectra as they appear in scattering and absorption experiments. A detailed analysis of line shapes, eigenfrequencies, and dynamical potential profiles within the layer reveals some new insight into nonlocal coupling mechanisms.

With decreasing temperature there is a continuous transition from an interface plasmon of the half-bound electron gas to a quasi-two-dimensional plasmon. At sufficiently low temperature we then studied effects of

nonlocality on the dispersion of both the plasmon and the collective mode of intersubband transitions. The well-known depolarization shift of this intersubband resonance at small $q_{\parallel}$ is shown to be strongly influenced by the spectral proximity of the continuum of states. The shift is only half of the value predicted by simple two-band models. At large wave-vector transfers the coupling between the two collective modes increases considerably.

So far there is no detailed experimental study of the dynamics of accumulation layers in the parameter regime, where $1/q_{\parallel}$ reaches the thickness of the inhomogeneity. We thus want to encourage high resolution inelastic electron scattering experiments (HRELS) on such quasi-two-dimensional systems. In addition to ZnO,[38] another suitable candidate for accumulations at the free surfaces required in HRELS might be indium arsenide.[39]

ACKNOWLEDGMENTS

The author would like to thank D. L. Mills and D. Heitmann for valuable discussions.

[1]R. Matz and H. Lüth, Phys. Rev. Lett. **46**, 500 (1981).
[2]A. Ritz and H. Lüth, Phys. Rev. Lett. **52**, 1242 (1984).
[3]A. Ritz and H. Lüth, J. Vac. Sci. Technol. B **3**, 1153 (1985).
[4]A. Förster and H. Lüth, Surf. Sci. **189-190**, 307 (1987).
[5]G. Abstreiter, M. Cardona, and A. Pinczuk, in *Light Scattering in Solids IV*, edited by M. Cardona and G. Güntherodt (Springer, Berlin, 1984).
[6]D. Heitmann and U. Mackens, Phys. Rev. B **33**, 8269 (1986).
[7]E. Batke, D. Heitmann, and C. W. Tu, Phys. Rev. B **34**, 6951 (1986).
[8]D. H. Ehlers and D. L. Mills, Phys. Rev. B **36**, 1051 (1987).
[9]For a review see T. Ando, A. B. Fowler, and F. Stern, Rev. Mod. Phys. **54**, 437 (1982).
[10]U. Gupta and A. K. Rajagopal, Phys. Rep. **87**, 259 (1982).
[11]R. G. Dandrea, N. W. Ashcroft, and A. E. Carlsson, Phys. Rev. B **34**, 2097 (1986).
[12]E. K. U. Gross and W. Kohn, Phys. Rev. Lett. **55**, 2850 (1985).
[13]T. Ando, J. Phys. Soc. Jpn. **51**, 3893 (1982).
[14]A. Gold, Phys. Rev. B **32**, 4014 (1985).
[15]G. A. Baraff and J. A. Appelbaum, Phys. Rev. B **5**, 475 (1972).
[16]D. H. Ehlers and D. L. Mills, Phys. Rev. B **34**, 3939 (1986).
[17]H. Ibach and D. L. Mills, *Electron Energy Loss Spectroscopy and Surface Vibrations* (Academic, San Francisco, 1982).
[18]M. V. Klein, in *Light Scattering in Solids*, 2nd ed., Vol. 8 of *Topics in Applied Physics*, edited by M. Cardona (Springer, Berlin, 1982).
[19]D. A. Dahl and L. J. Sham, Phys. Rev. B **16**, 651 (1977).
[20]Y. Takada, J. Phys. Soc. Jpn. **50**, 1998 (1981).
[21]D. L. Mills, Surf. Sci. **48**, 59 (1975).
[22]P. Hawrylak, Ji-Wei Wu, and J. J. Quinn, Phys. Rev. B **32**, 5169 (1985).
[23]B. N. J. Persson and E. Zaremba, Phys. Rev. B **31**, 1863 (1985).
[24]O. Madelung, M. Schulz, and H. Weiss, *Numerical Data and Functional Relationships in Science and Technology*, Vol. 17a of *Landolt-Börnstein*, edited by K. W. Hellwege (Springer, Berlin, 1982), Group 3.
[25]A. Griffin and J. Harris, Can. J. Phys. **54**, 1396 (1976).
[26]A. Pinczuk and J. M. Worlock, Surf. Sci. **113**, 69 (1982).
[27]P. Gies and R. R. Gerhardts, Phys. Rev. B **36**, 4422 (1987).
[28]A. Liebsch, Phys. Rev. B **36**, 7378 (1987).
[29]A. V. Chaplik Zh. Eksp. Teor. Fiz. **60**, 1845 (1971) [Sov. Phys.—JETP **33**, 997 (1971)].
[30]F. Stern, Phys. Rev. Lett. **14**, 546 (1967).
[31]T. K. Lee, C. S. Ting, and J. J. Quinn, Solid State Comm. **16**, 1309 (1975).
[32]J. I. Gersten, Surf. Sci. **97**, 206 (1980).
[33]S. Das Sarma, Phys. Rev. B **29**, 2334 (1984).
[34]R. Sooryakumar, A. Pinczuk, A. Gossard, and W. Wiegmann, Phys. Rev. B **31**, 2578 (1985).
[35]R. Z. Vitlina and A. V. Chaplik, Zh. Eksp. Teor. Fiz. **81**, 1011 (1981) [Sov. Phys.—JETP **54**, 536 (1981)].
[36]S. J. Allen, Jr., D. C. Tsui and B. Vinter, Solid State Commun. **20**, 425 (1976).
[37]J. K. Jain and S. Das Sarma, Phys. Rev. B **36**, 5949 (1987).
[38]J. I. Gersten, I. Wagner, A. Rosenthal, Y. Goldstein, A. Many, and R. E. Kirby, Phys. Rev. B **29**, 2458 (1984).
[39]J. M. Woodall, J. L. Freeouf, G. D. Pettit, T. Jackson, and P. Kirchner, J. Vac. Sci. Technol. **19**, 626 (1981).